Langmuir

Article

pubs.acs.org/Langmuir

Stepwise Molding, Etching, and Imprinting to Form Libraries of Nanopatterned Substrates

Zhi Zhao, Yangjun Cai, Wei-Ssu Liao, and Paul S. Cremer*

Department of Chemistry, Texas A&M University, College Station, Texas 77843, United States

Supporting Information

ABSTRACT: Herein, we describe a novel colloidal lithographic strategy for the stepwise patterning of planar substrates with numerous complex and unique designs. In conjunction with colloidal self-assembly, imprint molding, and capillary force lithography, reactive ion etching was used to create complex libraries of nanoscale features. This combinatorial strategy affords the ability to develop an exponentially increasing number of two-dimensional nanoscale patterns with each sequential step in the process. Specifically, dots, triangles, circles, and lines could be assembled on the surface separately and in combination with each other. Numerous architectures are obtained for the first time with high uniformity and reproducibility. These hexagonal arrays were made from polystyrene and gold features, whereby each surface element could be tuned from the micrometer size scale down to line widths of ~35 nm. The patterned area could be 1 cm^2 or even larger. The techniques described herein can be combined with further steps to make even larger libraries. Moreover, these polymer and metal features may prove useful in optical, sensing, and electronic applications.

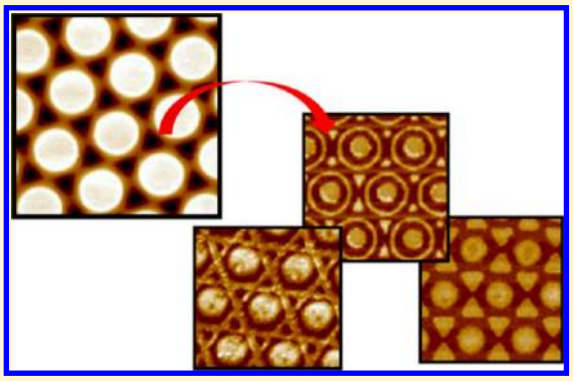

INTRODUCTION

Patterned arrays of metallic nanostructures are commonly used in photonics,[1,2] electronics,[3] material science,[4] and biotechnology[5−11] because of their unique electronic and optical properties. Much of this behavior results from surface plasmons, which represent the collective oscillation of conducting electrons on metal surfaces.[11] Multiple modes of surface plasmons, including localized surface plasmon resonance and propagating surface plasmon resonance, can be tuned in metal films as a function of structural and chemical properties. As a result, specific geometries and architectures are chosen and optimized for each application. For example, structures that are rich in edges or sharp crevices are believed to be useful for surface-enhanced Raman spectroscopy by providing hot spots of greater electromagnetic enhancement.[12,13] By contrast, the period and size of surface features are more essential for optical applications, which require a precise match between external excitation fields and surface plasmon modes.[14,15] The ability to create a library of surface structures through a combinatorial patterning technique would be highly desirable for screening the most efficient structures for a given individual purpose.

Great effort has been devoted to developing patterning methods that meet the exacting requirements of shape, size, orientation and periodicity for generating nanoscale platforms. This includes, among others, colloidal lithography, photolithography, soft lithography, and scanning beam lithography approaches.[16] The advantage of these methods is that they afford high reproducibility and good control over surface morphology. Despite their success, there are still substantial barriers for achieving very fine scale structures and complex designs over macroscopic areas in a reasonable time period. In principle, it is possible to fabricate almost any arbitrary feature with 10 nm resolution or better by electron beam lithography (EBL)[17−19] or focused ion beam lithography (FIB).[20] Nevertheless, the amount of time and cost rises tremendously as the patterned area increases and the features become more complex. By contrast, more rapid methods such as photolithography (PL)[21] readily allow for the fabrication of complex structures over large areas but have more difficulty producing very small objects due to the diffraction limit. Patterning methods including colloidal lithography (CL)[22,23] and soft lithography[24] generally meet the resolution, large area, cost, and time requirements. However, the types of features that can easily be produced are typically much more limited. As such, CL and soft lithography approaches are often combined with PL or EBL in order to fabricate fine surface features,[25−28] although some of the inherent disadvantages remain in place.

To expand the variety of architectures that can be inexpensively and rapidly fabricated, additional methods need to be pursued that can provide both large area patterning and small feature sizes. One idea would be to employ a stepwise or combinatorial approach for creating large libraries of patterns. The key is to incorporate steps that do not require PL, EBL,

Received: March 12, 2013
Revised: May 3, 2013
Published: May 17, 2013

   dx.doi.org/10.1021/la400943j | Langmuir 2013, 29, 6737−6745

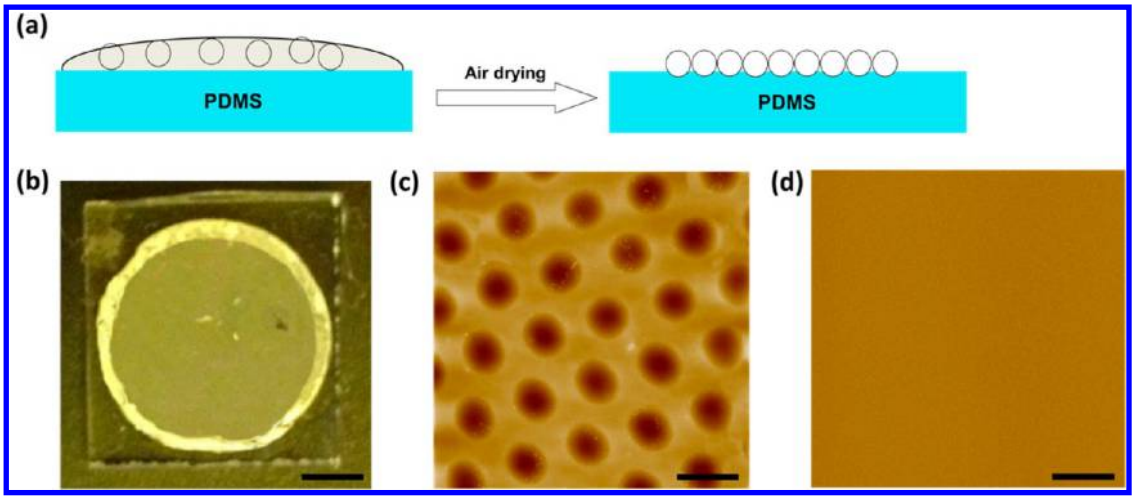

Figure 1. (a) Schematic diagram for forming a PS sphere monolayer. (b) Optical image of the self-assembled PS sphere layer on PDMS. Scale bar: 2 mm. (c) Tapping-mode AFM image of the PDMS surface after removal of the PS sphere monolayer in which the PDMS is cured for 3 h at 70 °C. Scale bar: 2 μm. (d) AFM image of the PDMS surface after removal of the PS sphere monolayer whereby the PDMS is cured for 24 h at 70 °C. Scale bar: 2 μm. Panels c and d are in the same height scale.

and FIB and, therefore, do not slow the process down or require specialized facilities and high costs. As a step toward realizing this goal, we introduce a colloidal lithography method to create complicated architectures in a poly(dimethylsiloxane) (PDMS) template through a combination of self-assembly, molding, and reactive ion etching (RIE). By integrating PDMS templating with capillary force lithography,[29] a large number of patterns could be generated in a polystyrene (PS) layer. An even greater variety of gold (Au) features could then be generated by tuning the time employed for oxygen plasma etching of the PS layer, which was followed by wet chemical etching to transfer the pattern to an underlying thin Au film. By doing this, dots, triangles, circles, lines, and related patterning units could be formed individually or in combination with each other. Each surface element could be tuned from the micrometer scale to well below the 100 nm level, while the size of the patterned area was about 1 cm^2.

EXPERIMENTAL SECTION

Formation of the Polystyrene Sphere Monolayer. PS beads of certified size standards were purchased from Duke Scientific Corp. with diameters of 400 nm, 800 nm, and 2 μm. The beads were centrifuged five times with copious amounts of water to remove surfactants and other impurities that were present from the manufacturer. They were then redissolved in purified water (Barnstead nanopure water system, 18 MΩ·cm resistivity). The concentration of PS spheres was maintained at $4 \times 10^7/\mu$L for all sizes. Triton X-100, laboratory-grade, was purchased from Sigma–Aldrich. PS bead suspensions were mixed with a 0.1% (volume percentage) Triton X-100 solution in a 4:1 ratio to yield a final surfactant concentration of 0.020 vol %. PDMS molds were made by mixing Sylgard 184 silicone elastomer with 10 wt % Sylgard 184 curing agent. The mixture was then cured at 70 °C for 3 h. Before the aqueous PS sphere suspension was introduced, the PDMS surface was treated with oxygen plasma for 15 s to increase its hydrophilicity. The PDC-32G plasma cleaner/sterilizer was from Harrick Plasma (Ithaca, NY).

Poly(dimethylsiloxane) Templates. A March CS-1701 reactive ion etcher was used to create PDMS templates. To do this, a PDMS film coated with a monolayer of PS spheres was exposed to carbon tetrafluoride (CF_4)/oxygen (O_2) plasma at 270 W in the reactive ion etcher for varying time periods. The total flow rate of the etchant was kept at 40 standard cubic centimeters per minute (sccm) while the etchant composition was varied for creating various pillar spacings. After treatment, the PS spheres were removed from the PDMS surface by sonication first in toluene followed by acetone and water. Toluene was bought from EMD, and acetone was purchased from Fisher Scientific; both were ACS-grade. PDMS template was heated under 130 °C for 30 min to further remove any absorbed solvent before use.

Polystyrene and Gold Features. Glass slides (VWR, no. 2 micro cover slides) were treated with piranha solution to remove organics from the surface. This solution was a 3:1 mixture of sulfuric acid (EMD, ACS grade) and hydrogen peroxide (Acros Organics, 35%) (caution: piranha solutions are extremely corrosive, reactive, potentially explosive, and need to be handled with care in a fume hood). The glass slides were then washed with water and baked in an oven (Orton, Sentry Xpress 2.0) at 500 °C for 5 h. A 50 nm thick Au layer (Alfa Aesar, 99.999%) was thermally evaporated onto the glass slides by use of a 5 nm thick chromium layer as an adhesive. This was done in a BOC Edwards metal evaporator (Auto 360). Polystyrene powder (Scientific Polymer, MW = 97 400) was first dissolved in toluene and then spin-coated onto the planar Au surface by use of a WS-400B-6NPP/LITE spin coater (Laurell Techonologies Corp.). The spinning rate was set to 3000 rpm/min, while the concentration of the PS solution was tuned between 5 and 50 mg/mL depending on the thickness of the PS film that was desired. Detailed parameters for the setup can be found in Table S2 (Supporting Information).

The PDMS template was placed on a polymer layer and an iron block was used to adjust the applied pressure. The applied pressure was set to $\sim 7.9 \times 10^3$ Pa by placing an 80 g iron block on a 1 cm × 1 cm PDMS mold. Next, the system was annealed at 130 °C for time periods ranging from 30 min to 1 h and then cooled back to room temperature in air. After the PDMS layer was peeled away, the nascently formed polymer features were treated in an oxygen plasma to completely remove the thinnest portions of the PS film. The power of the RIE was set to 60 W and the oxygen flow rate was 20 sccm, which initially corresponded to a removal rate of 2 nm/s. Finally, the whole chip was immersed in a mixture of 50 mM iron nitrate (Alfa Aesar, 98+%) and 50 mM thiourea (Alfa Aesar, 99%). After removal of the unprotected Au, the chip was rinsed with purified water and treated with chromium etchant 1020 (Transene Company Inc.) for 1 min to dissolve the exposed chromium. The remaining PS layer was removed by toluene before each gold feature was examined by atomic force microscopy (AFM; Digital Instrument, multimode scanning probe microscope) in tapping mode to explore the surface topography.

RESULTS AND DISCUSSION

Our patterning procedure consisted of consecutive colloidal lithography and reactive ion etching steps. To do this, a flat

dx.doi.org/10.1021/la400943j | Langmuir 2013, 29, 6737–6745

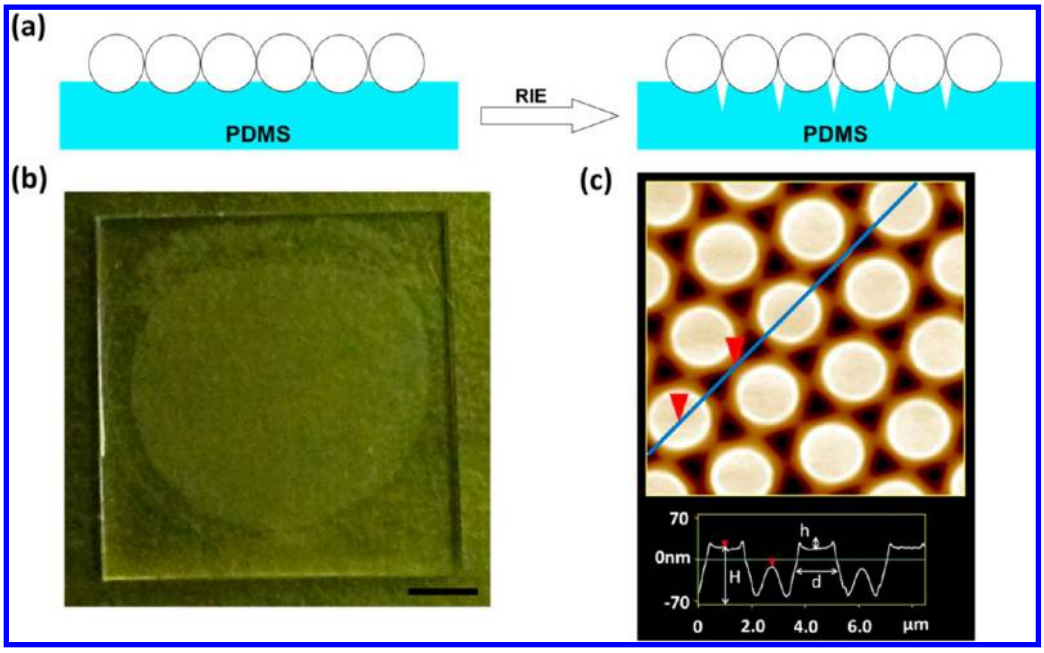

Figure 2. (a) Schematic diagram of the binary reactive ion etching step. (b) Optical image of the PDMS template after RIE and removal of the PS sphere monolayer. Scale bar: 2 mm. (c) Representative view of the surface of the PDMS template, with a height profile shown beneath it.

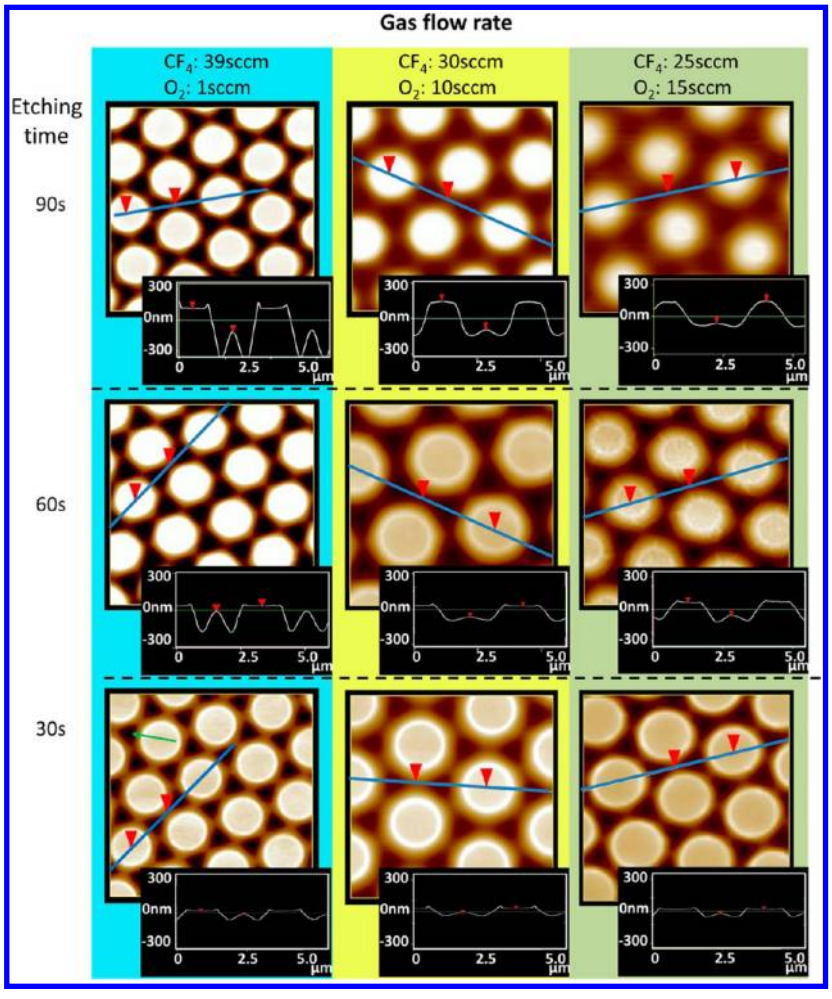

Figure 3. AFM images and line profiles of the PDMS molds with various O_2:CF_4 ratios and etching times. A 3-fold hollow site is pointed out in the lower-left image by a green arrow. The red arrowheads in each image denote positions along the line profile over the blue line. Each line profile is displayed as an inset.

dx.doi.org/10.1021/la400943j | *Langmuir* 2013, 29, 6737−6745

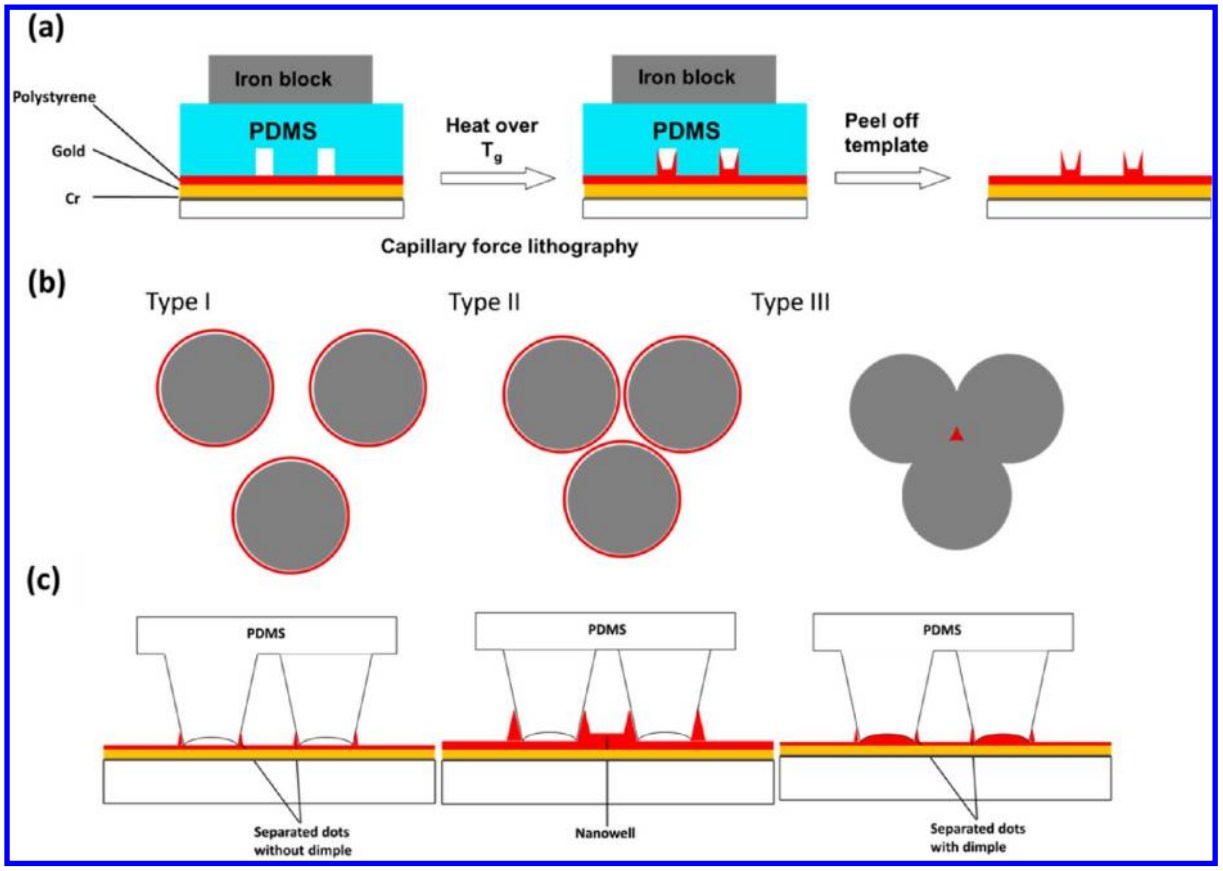

Figure 4. (a) Schematic diagram of the layered substrate used in capillary force lithography and the procedure for creating PS patterns. (b) Schematic diagrams of the three types of spacings for PDMS pillars. (c) Schematic diagrams showing the influence of PS film thickness (in red) and annealing times on the PS film structures obtained. (Left) Features formed by using a thinner film with a 30 min annealing time; (middle) features formed by using a thicker film with a 30 min annealing time; (right) features formed by using a thinner film with a 60 min annealing time.

PDMS substrate was cured at 70 °C for 3 h. It was then rendered partially hydrophilic in O_2 plasma and used immediately. Next, a monolayer of polystyrene (PS) spheres was assembled via deposition from an aqueous suspension onto the planar PDMS surface.[30−32] The spheres had a diameter of 2 μm and formed a closely packed hexagonal monolayer on the surface upon evaporation of the water solution (Figure 1a). This process typically took ∼2 h. It should be noted that a close-packed self-assembled monolayer of PS spheres on PDMS has not been previously demonstrated. These experimental conditions represented a significant modification of deposition techniques previously employed to deposit PS spheres on glass or silicon substrates.[33,34] Specifically, the production of PDMS surfaces of intermediate hydrophobicity was the key to forming a high-quality self-assembled colloidal sphere monolayer. Moreover, introduction of 0.020 vol % Triton X-100 to the deposited aqueous droplet facilitated the formation of a uniform single monolayer. For these experiments, a contact angle for water of ∼40° with the PDMS worked well. To obtain this degree of hydrophobicity, the elastomeric substrate was treated in 18 W O_2 plasma for 15 s with initial O_2 pressure of 0.1 bar. When the PDMS surface was made more hydrophobic, it led to colloidal multilayer formation. By contrast, when it was made more hydrophilic, increasing disorder in the colloidal array was found. The area that could be patterned with PS spheres depended on the total volume of liquid solution that was introduced onto the PDMS surface. In particular, a coating with approximately 1 cm diameter could be made by introducing a 30 μL volume solution. An optical image of the dried film is shown in Figure 1b. As can be seen, the film was thicker near the rim, but otherwise a single monolayer was achieved.

The colloidal sphere layer created a dimple array in the underlying PDMS substrate when left in contract with the substrate overnight. To demonstrate this, the PS spheres could be removed and the substrate subsequently imaged. Removal was performed by sonication in a bath with a 50/50 volume mixture of acetone and water for 1 min. The PDMS slab was then washed with water and dried in flowing nitrogen. AFM imaging revealed that an array of dimples was formed in the PDMS surface (Figure 1c). If we employed PDMS that was cured at 70 °C for 24 h instead of 3 h and kept other conditions the same, no dimple array pattern was found after sonication (Figure 1d). As such, it is believed that un-cross-linked PDMS strands are keys to forming the dimples by molding around the PS spheres after assembly. Also, this molding process did not occur immediately, as removal of the colloidal array by sonication only a few minutes after the self-assembly process was completed did not leave the dimple pattern behind.

In a next step, a PS sphere-covered PDMS substrate was subjected to plasma etching (Figure 2a). The etchant in the RIE procedure consisted of a 39:1 mixture of CF_4 and O_2.[35] The total flow rate was 40 sccm at a pressure of 80 mTorr. Etching was conducted for 30 s with a 270 W plasma. The reactivity of PDMS and PS are quite different for these two gases. The Si−O backbone of PDMS primarily reacted with $F^{\bullet}$,

dx.doi.org/10.1021/la400943j | *Langmuir* 2013, 29, 6737−6745

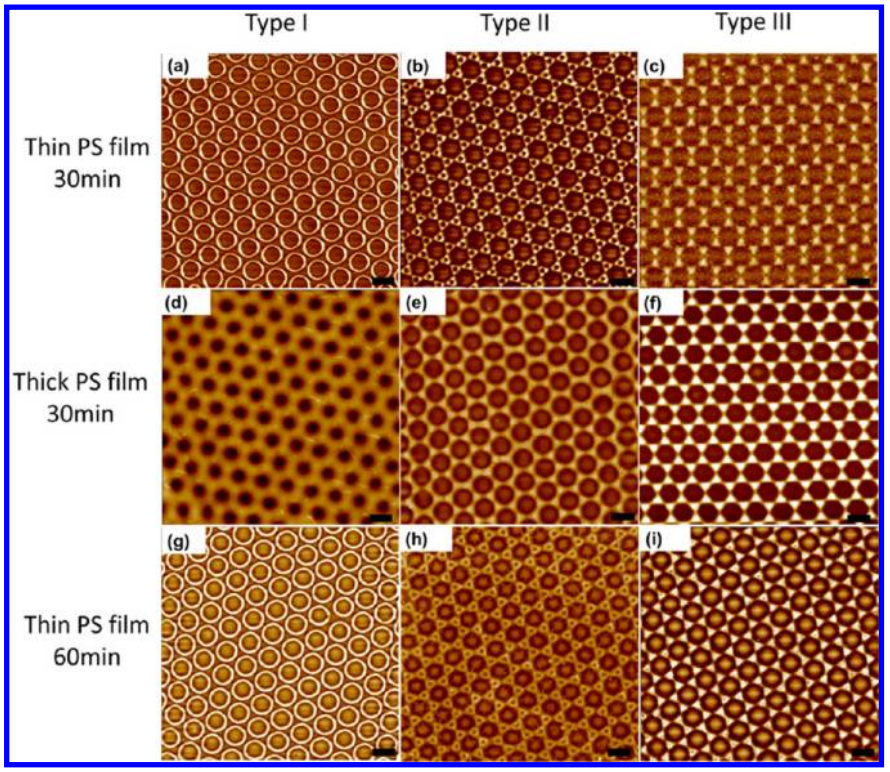

Figure 5. Various PS patterns obtained by adjusting the PS film thickness and annealing time. Scale bars: 2 μm.

while the PS was relatively stable in $F^{\bullet}$.[35,36] Only the PDMS surface that was not shielded by the PS spheres was etched, which led to a hexagonal array of pillars. After the pattern was formed, the PS spheres were dissolved with toluene and the PDMS template was cleaned by acetone and water. An optical image of the entire substrate after this procedure is shown in Figure 2b. The sample could then be imaged microscopically by AFM. This revealed that an array of PDMS pillars was formed (Figure 2c). The hexagonal pillar array was characterized by height of the PDMS pillars (H), depth of the indent on top of the pillars (h), width of the pillars at half height (d), and periodicity of the pillar array. The period was determined by the original size of PS spheres, while all the other parameters could be tuned in a very broad range by controlling the RIE time, O_2 concentration, and size of the PS spheres.

The relative amount of O_2 was the most essential parameter for tuning the features of the pillar array (Figure 3). Indeed, varying the concentration of O_2 drastically changed the morphology of the PS sphere mask. As is well-known, the C−C backbone of PS can be etched quickly in oxygen.[37] As a result, we could partially oblate the PS spheres by adding more oxygen to the etchant gas. This served to uncover more of the PDMS surface. Depending on the etching conditions, the PS sphere diameter could be tuned to leave the spheres touching or widely separated. Since the underlying PDMS substrate was simultaneously being etched by CF_4 (and to a lesser extent by O_2), the resulting pattern in the underlying substrate would change. The total flow rate of etchant was kept constant at 40 sccm at a total pressure of 80 mTorr under all conditions. AFM images of the surface topography of the patterned PDMS surface after etching with various O_2:CF_4 ratios and etching times are shown in Figure 3. The images were taken after subsequent removal of the PS spheres by dissolving them with toluene. As can be seen, increasing the ratio of O_2 to CF_4 (left to right) created more room between the pillars. On the other hand, increasing the time of plasma etching create deeper valleys in the PDMS (bottom to top images).

A hexagram pattern was formed in the 3-fold hollow sites between the locations of the PS spheres under conditions where the $O^{\bullet}$ concentration was relatively low. This can be seen by the dark triangular regions in the lower left-hand image (green arrow in Figure 3). As the oxygen ratio was increased, the etching rate of the spheres increased relative to that of the PDMS substrate. This led to bridge-shaped dips descending between adjacent spheres. As a result, the height difference between the top of the pillars and the top of the bridges became larger as the etching time increased. Moreover, the triangular regions became deeper and the diameter of the spherical pillars became smaller as the etching time was increased under all conditions. Depending on the plasma etching time, the pillars in the PDMS templates could be defined as well separated (type I), closely separated (type II), or overlapping (type III) based on the interpillar separation. This classification is reflected in the top, middle, and bottom rows of images in Figure 3, respectively.

Next, the patterned PDMS substrates were used to create arrays of complex nanoscale features in both PS and Au thin films. The system used for these experiments consisted of a 10−50 nm PS layer, which was spin-coated onto a 50 nm thick Au layer on a planar glass substrate. An intervening 5 nm Cr layer was used to wet the Au uniformly onto the glass (Figure 4a). It should be noted that each PDMS template was copiously washed with both water and organic solvents before proceeding to the next step (see Experimental Section for details). As a result, most traces of PS and Triton X-100 should be absent after patterning.

The PS layer was patterned first by capillary force lithography.[29,38] To do this, the PDMS mold was placed onto

dx.doi.org/10.1021/la400943j | Langmuir 2013, 29, 6737−6745

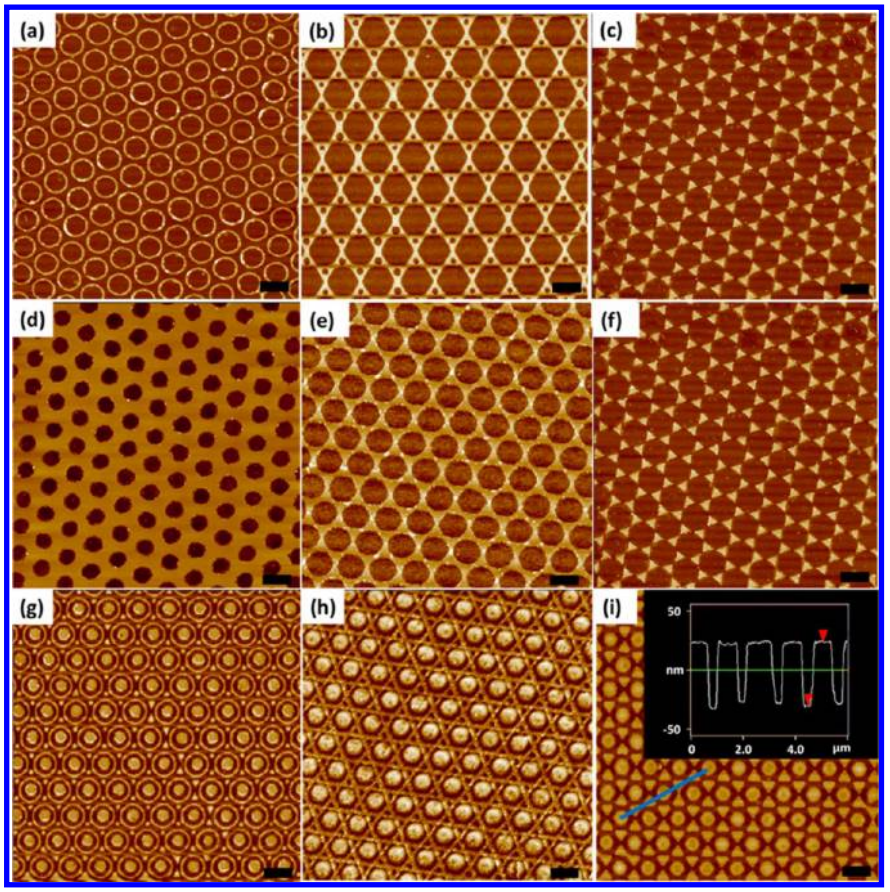

Figure 6. Au nanopatterns created from the respective PS templates in Figure 5. (a–h) Various gold features. Scale bars: 2 μm. (i) Triangle-dot gold feature. The height information of the region under the blue line is displayed in the inset. Scale bar: 2 μm.

a polystyrene-coated planar glass substrate. An iron block was placed on top of the mold to ensure close contact between the mold and the polymer as well as to adjust the pressure applied to the substrate. The whole system was then heated for a fixed period of time at 130 °C, which was above the glass transition temperature (T_g) of PS.[39] PS features were formed as the polymer melt climbed up the walls under the influence of capillary forces.[29,40] As the temperature rose above T_g, the PS layer was melted and accumulated around the edge of the PDMS pillars. This kind of capillary rise was mainly driven by surface tension as the initial contact angle between the PDMS walls and the PS layer was 90°, which is far from the equilibrium contact angle (~76°).[29,40]

Distinct patterns in the PS layer could be generated by changing the pillar spacing (Figure 4b) and by varying the heating time and PS layer thickness (Figure 4c). For example, when the width of capillary rise was smaller than the gap (g) between adjacent PDMS pillars (type I), circular rings were generated (Figure 4b, left). The PS film employed here was ~20 nm thick and a heating time of 30 min was used. If the gap between the pillars was reduced to a range comparable to the size of the PS features (type II template), connected structures such as hexagrams were formed in the PS surface (Figure 4b, middle). The film thickness in this case was 12 nm for optimized overlap. Finally, if only a small portion of the 3-fold hollow site was etched (type III), triangular hexagram structures were formed by use of 10 nm thick PS films (Figure 4b, right). The red outlines in Figure 4b denote filling regions into which PS material would flow around the circular pillars (gray). In particular, those three conditions correspond to PS patterns in Figure 5a–c, respectively.

As noted above, the PS film thickness was a critical parameter, with a greater capillary rise occurring for thicker films. For example, if one increased the PS film from 20 to 30 nm and kept other parameters identical, nanowells were generated instead of rings for type I conditions (Figure 5d). Indeed, the thicker PS film more completely filled the voids in the template compared with Figure 5a. Similarly, hexagonal wells were formed by using a type II template and a 15 nm PS film (Figure 5, panel e versus panel b). Such differences, however, were smaller with type III features, as the void space in the PDMS molds was considerably smaller (Figure 5, panel f versus panel c).

In addition to the patterns described above, it was found that the heating time of the PS layer also played an important role. In fact, a central dimple could be introduced by increasing this time to ~1 h from ~30 min under otherwise identical conditions. This is shown in Figure 5g–i, which correspond to Figure 5a–c, respectively. Apparently, PS was initially excluded from rising into the indented portion of the pillars over the first 30 min of the capillary rise process. After 60 min, however, the polymer melt filled this region too. This time-dependent annealing feature may be related to gas trapped between the top of the PDMS pillars and the PS layer that initially prevents dimple formation. The influence of both film thickness and heating time on the molding of PS features is illustrated schematically in Figure 4c.

dx.doi.org/10.1021/la400943j | *Langmuir* 2013, 29, 6737–6745

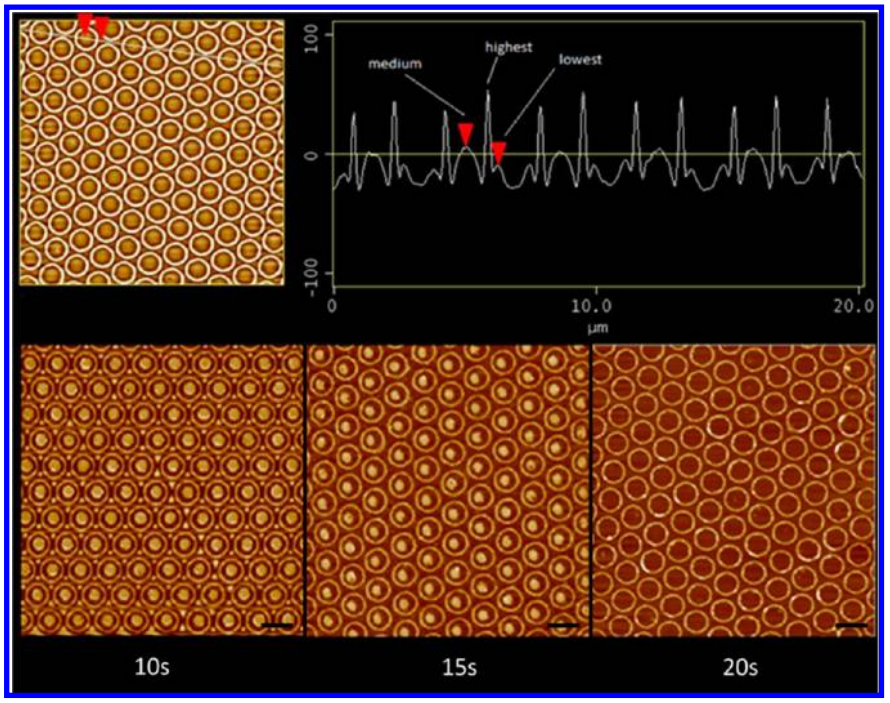

Figure 7. Three Au patterns (bottom row) fabricated from the same PS template (upper-left image) by control of the etching time in RIE. The etching time is listed under each image. The period for the patterns is 2 μm, and a line profile is shown next to the PS template. Scale bars: 2 μm.

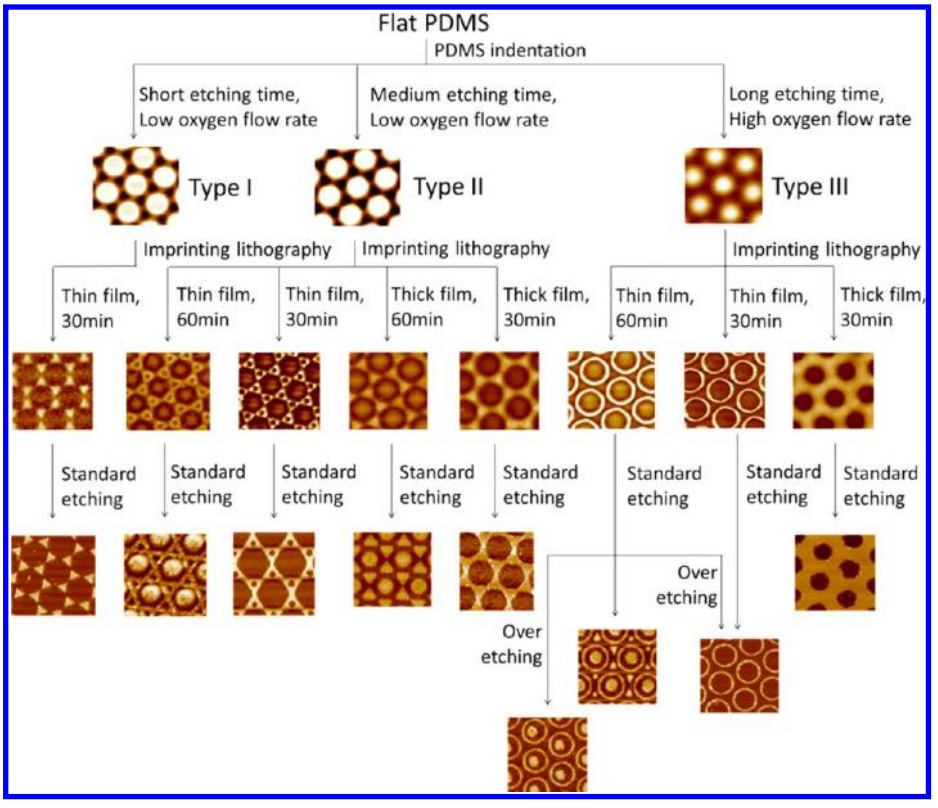

Figure 8. Branching tree guide to the strategies employed for fabricating various Au pattern motifs by the stepwise templating method. All patterns shown here have 2 μm periodicity.

Finally, the PS patterns could also be transferred into an underlying Au layer. This was done by treating the PS pattern with an oxygen plasma for a fixed amount of time in order to expose the desired parts of the metal layer. Then the chip was immersed into a 1:1 (volumetric) mixture of 50 mM ferric nitrate and 50 mM thiourea to conduct a wet chemical etch. After removal of the exposed Au, the chip was treated with chromium etchant for 1 min to dissolve the subsequently exposed chromium adhesion layer beneath the Au film. Finally, the chip was washed with toluene and copious amounts of acetone and deionized water to remove the polymer layer.

dx.doi.org/10.1021/la400943j | *Langmuir* 2013, 29, 6737−6745

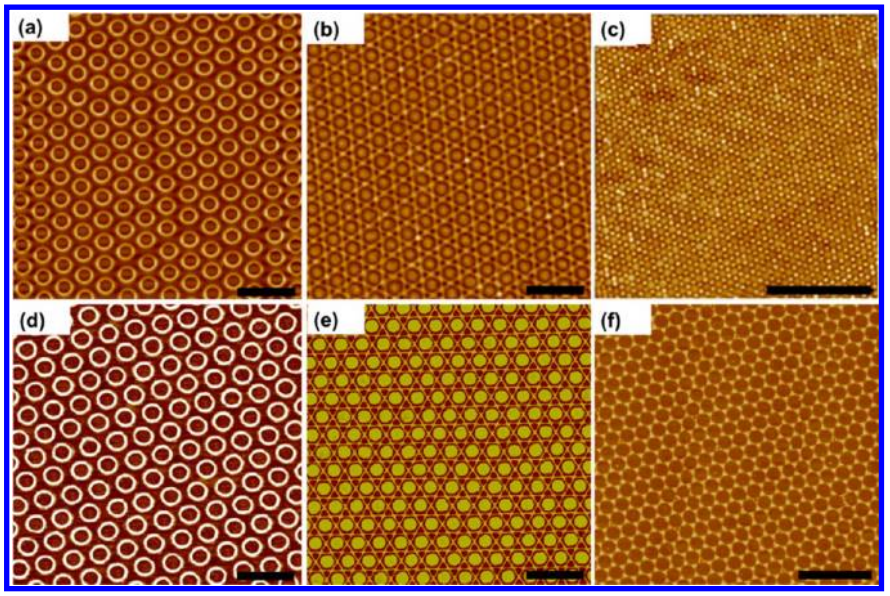

Figure 9. PS thin film features created with (a, b) 800 nm and (c) 400 nm PS spheres. Type I features are shown in panel a, while type II features are shown in panel b. (d–f) Corresponding Au features generated from the PS templates in pnaels a–c. Scale bars: 2 μm.

In order to faithfully transfer the polymer features into the Au film, the plasma etching time was carefully controlled so that only the planar portions of the polymer layer were removed, while the raised areas were left behind. This was done by adjusting the plasma etching time. The plasma etching speed was approximately 2 nm/s under our conditions. Therefore, the amount of PS that was ultimately removed was easy to control. The resulting Au layer patterns are shown in Figure 6. Each image in the 3 × 3 array corresponds to its PS template in Figure 5. For example, Figure 6a was obtained by using the PS pattern in Figure 5a. As can be seen, a rich variety of Au patterns can be created. This includes rings, triangles, targets, wells, lines, and complex combinations of these features. Many of these large-scale Au patterned elements should be unique to this patterning method, including the hexagonal web (Figure 6b), the targets surrounding by triangles (Figure 6g), and hexagonal web with dots (Figure 6h). The height of gold features shown here is equal to 55 ± 5 nm, which was obtained from AFM measurements and demonstrated typically in Figure 6i. This number is coincident with the total thickness of deposited gold (50 nm) and Cr (5 nm) layers. It is also possible to develop an even richer array of Au patterns by varying the etching time of the PS film. For example, the removal of some of the raised portions of the PS pattern can be achieved by overetching. As a result, the gold patterns can have different topologies from the original PS templates. Figure 7 shows three distinct Au patterns made from the same PS template by varying the plasma etching time. The original PS pattern was composed of three moieties with different heights: small triangular dots, dimples, and ring structures. The triangles were thinnest, while the rings were the tallest features as shown by a line scan of the PS template (Figure 7, top image and corresponding line scan). By use of a minimum etching time (10 s), all features were preserved in the Au layer including the small triangles, while a longer etching time left just the rings (20 s). An intermediate etching time (15 s) removed the small triangles but not the center dot (Figure 7, three lower images, left to right). Exact details for the etching times and other fabrication conditions are provided in Table S1 (Supporting Information). The height of gold features shown here is equal to 55 ± 5 nm.

The most significant advantage of our method is that one can make a very large variety of patterns. A branching tree is provided to summarize the conditions for creating specific motifs (Figure 8). In fact, the ability of our method to fabricate different feature types and patterns in Au is even greater than what is shown here. Indeed, since the RIE gas composition, plasma etching time, capillary force lithography time, PS film thickness, and Au etching time can each be controlled separately, a very large library of distinct features can be formed. Moreover, the patterning method described above was performed with 2 μm colloidal spheres. The size of these spheres, of course, can be varied as well to change the element size and spacing. In fact, we have repeated these methods with 800 and 400 nm PS spheres. In the latter case, the line widths of the PS features were about 35 nm (Figure 9). Again, the height of gold features shown here is equal to 55 ± 5 nm.

■ CONCLUSIONS

We have developed a novel strategy to establish libraries of surface patterns. The approach used a combination of colloidal lithography, reactive ion etching, and soft lithography for patterning a thin PS layer, followed by etching an Au layer. Indeed, a wide variety of PS and Au patterns were fabricated on the micrometer scale and nanoscale. Unique and complex metal features, such as hexagonal webs and targets with triangles, could be created by simply choosing a proper template and PS layer thicknesses. Such complex nanoscale features patterned over large areas would be difficult to create by other methods.

■ ASSOCIATED CONTENT

Ⓢ Supporting Information

Two tables listing detailed fabrication conditions of PS and Au nanofeatures. This material is available free of charge via the Internet at http://pubs.acs.org.

dx.doi.org/10.1021/la400943j | *Langmuir* 2013, 29, 6737–6745

AUTHOR INFORMATION

Corresponding Author

*E-mail cremer@chem.tamu.edu.

Notes

The authors declare no competing financial interest.

ACKNOWLEDGMENTS

This work was supported by a Norman Hackerman Advanced Research Project Program grant (010366-0040-2009) and by the Office of Naval Research (N00014-08-0467).

REFERENCES

(1) Joannopoulos, J. D.; Villeneuve, P. R.; Fan, S. H. Photonic crystals: putting a new twist on light. *Nature* **1997**, *386*, 143−149.

(2) Joannopoulos, J. D.; Meade, R. D.; Winn, J. N. *Photonic Crystals: Modeling the Flow of Light*; Princeton University Press: Princeton, NJ, 1995.

(3) Jacobs, H. O.; Whitesides, G. M. Submicrometer patterning of charge in thin-film electrets. *Science* **2001**, *291*, 1763−1766.

(4) Thurn-Albrecht, T.; Schotter, J.; Kastle, C. A.; Emley, N.; Shibauchi, T.; Krusin-Elbaum, L.; Guarini, K.; Black, C. T.; Tuominen, M. T.; Russell, T. P. Ultrahigh-density nanowire arrays grown in self-assembled diblock copolymer templates. *Science* **2000**, *290*, 2126−2129.

(5) Haes, A. J.; Van Duyne, R. P. A nanoscale optical biosensor: sensitivity and selectivity of an approach based on the localized surface plasmon resonance spectroscopy of triangular silver nanoparticles. *J. Am. Chem. Soc.* **2002**, *124*, 10596−10604.

(6) Ostuni, E.; Chen, C. S.; Ingber, D.; Whitesides, G. M. Selective deposition of proteins and cells in arrays of microwells. *Langmuir* **2001**, *17*, 2828−2834.

(7) Lee, K. B.; Park, S. J.; Mirkin, C. A.; Smith, J. C.; Mrksich, M. Protein nanoarrays generated by dip-pen nanolithography. *Science* **2002**, *295*, 1702−1705.

(8) Kohli, P.; Harrell, C. C.; Cao, Z.; Gasparac, R.; Tan, W.; Martin, C. R. DNA-functionalized nanotube membranes with single-base mismatch selectivity. *Science* **2004**, *305*, 984−986.

(9) Chan, W. C. W.; Nie, S. Quantum dot bioconjugates for ultrasensitive nonisotopic detection. *Science* **1998**, *281*, 2016−2018.

(10) Han, M.; Gao, X.; Su, J. Z.; Nie, S. Quantum-dot-tagged microbeads for multiplexed optical coding of biomolecules. *Nat. Biotechnol.* **2001**, *19*, 631−635.

(11) Ebbesen, T. W.; Lezec, H. J.; Ghaemi, H. F.; Thio, T.; Wolff, P. A. Extraordinary optical transmission through sub-wavelength hole arrays. *Nature* **1998**, *391*, 667−669.

(12) Xu, H.; Bjerneld, E. J.; Käll, M.; Börjesson, L. Spectroscopy of single hemoglobin molecules by surface enhanced Raman scattering. *Phys. Rev. Lett.* **1999**, *83*, 4357−4360.

(13) Xu, H.; Aizpurua, J.; Käll, M.; Apell, P. Electromagnetic contributions to single-molecule sensitivity in surface-enhanced Raman scattering. *Phys. Rev. E* **2000**, *62*, 4318−4324.

(14) Link, S.; El-Sayed, M. A. Size and temperature dependence of the plasmon absorption of colloidal gold nanoparticles. *J. Phys. Chem. B.* **1999**, *103*, 4212−4217.

(15) Gao, H.; McMahon, J. M.; Lee, M. H.; Henzie, J.; Gray, S. K.; Schatz, G. C.; Odom, T. W. Rayleigh anomaly-surface plasmon polariton resonances in palladium and gold subwavelength hole arrays. *Opt. Express* **2009**, *17*, 2334−2340.

(16) Stewart, M. E.; Anderton, C. R.; Thompson, L. B.; Maria, J.; Gray, S. K.; Rogers, J. A.; Nuzzo, R. G. Nanostructured plasmonic sensors. *Chem. Rev.* **2008**, *108*, 494−521.

(17) Rechberger, W.; Hohenau, A.; Leitner, A.; Krenn, J. R.; Lamprecht, B. F.; Aussenegg, R. Optical properties of two interacting gold nanoparticles. *Opt. Commun.* **2003**, *220*, 137−141.

(18) Grand, J.; Adam, P. M.; Grimault, A. S.; Vial, A.; de la Chapelle, M. L.; Bijeon, J. L.; Kostcheev, S.; Royer, P. Optical extinction spectroscopy of oblate, prolate and ellipsoid shaped gold nanoparticles: experiments and theory. *Plasmonics* **2006**, *1*, 135−140.

(19) Duan, H.; Hu, H.; Kumar, K.; Shen, Z.; Yang, J. Direct and reliable patterning of plasmonic nanostructures with sub-10-nm gaps. *ACS Nano* **2011**, *5*, 7593−7600.

(20) Ohno, T.; Bain, J. A.; Schlesinger, T. E. Observation of geometrical resonance in optical throughput of very small aperture lasers associated with surface plasmons. *J. Appl. Phys.* **2007**, *101*, No. 083107.

(21) Moreau, W. M. *Semiconductor Lithography*; Plenum: New York, 1989.

(22) Haynes, C. L.; Van Duyne, R. P. Nanosphere lithography: a versatile nanofabrication tool for studies of size-dependent nanoparticle optics. *J. Phys. Chem. B* **2001**, *105*, 5599−5611.

(23) Geng, C.; Zheng, L.; Yu, J.; Yan, Q.; Wei, T.; Wang, X.; Shen, D. Thermal annealing of colloidal monolayer at the air/water interface: a facile approach to transferrable colloidal masks with tunable interstice size for nanosphere lithography. *J. Mater. Chem.* **2012**, *22*, 22678−22685.

(24) Xia, Y.; Whitesides, G. M. Soft lithography. *Angew. Chem., Int. Ed.* **1998**, *37*, 550−575.

(25) Huang, Y.; Paloczi, G. T.; Yariv, A.; Zhang, C.; Dalton, L. R. Fabrication and replication of polymer integrated optical devices using electron-beam lithography and soft lithography. *J. Phys. Chem. B* **2004**, *108*, 8606−8613.

(26) Kim, Y. H.; Park, J.; Yoo, P. J.; Hammond, P. T. Selective assembly of colloidal particles on a nanostructured template coated with polyelectrolyte multilayers. *Adv. Mater.* **2007**, *19*, 4426−4430.

(27) Li, X.; Peter, M.; Huskens, J.; Reinhoudt, D. N. Catalytic microcontact printing without ink. *Nano Lett.* **2003**, *3*, 1449−1453.

(28) Chen, J. Y.; Klemic, J. F.; Elimelech, M. Micropatterning microscopic charge heterogeneity on flat surfaces for studying the interaction between colloidal particles and heterogeneously charged surfaces. *Nano Lett.* **2002**, *2*, 393−396.

(29) Suh, K. Y.; Kim, Y. S.; Lee, H. H. Capillary force lithography. *Adv. Mater.* **2001**, *13*, 1386−1389.

(30) Deegan, R. D.; Bakajin, O.; Dupont, T. F.; Huber, G.; Nagel, S. R.; Witten, T. A. Capillary flow as the cause of ring stains from dried liquid drops. *Nature* **1997**, *389*, 827−829.

(31) Deegan, R. D. Pattern formation in drying drops. *Phys. Rev. E* **2000**, *61*, 475−485.

(32) Deegan, R. D.; Bakajin, O.; Dupont, T. F.; Huber, G.; Nagel, S. R.; Witten, T. A. Contact line deposits in an evaporating drop. *Phys. Rev. E* **2000**, *62*, 756−765.

(33) Wang, X.; Summers, C. J.; Wang, Z. Large-scale hexagonal-patterned growth of aligned ZnO nanorods for nano-optoelectronics and nanosensor arrays. *Nano Lett.* **2004**, *4*, 423−426.

(34) Huang, Z. P.; Carnahan, D. L.; Rybczynski, J.; Giersig, M.; Sennett, M.; Wang, D. Z.; Wen, J. G.; Kempa, K.; Ren, Z. F. Growth of large periodic arrays of carbon nanotubes. *Appl. Phys. Lett.* **2003**, *82*, 460−462.

(35) Garra, J.; Long, T.; Currie, J.; Schneider, T.; White, R.; Paranjape, M. Dry etching of polydimethylsiloxane for microfluidic systems. *J. Vac. Sci. Technol. A* **2002**, *20*, 975−982.

(36) Glocker, D. A.; Shah, S. I. *Handbook of Thin Film Process Technology*; Institute of Physics: Bristol, U.K., 1995.

(37) Plettl, A.; Enderle, F.; Saitner, M.; Manzke, A.; Pfahler, C.; Wiedemann, S.; Ziemann, P. Non-close-packed crystals from self-assembled polystyrene spheres by isotropic plasma etching: adding flexibility to colloid lithography. *Adv. Funct. Mater.* **2009**, *19*, 3279−3284.

(38) Zhang, H.; Bucknall, D. G.; Dupuis, A. Uniform nanoscopic polystyrene patterns produced from a microscopic mold. *Nano Lett.* **2004**, *4*, 1513−1519.

(39) Mark, J. E. *Polymer Data Handbook*, 2nd ed.; Oxford University Press: Oxford, England, 2009.

(40) Cai, Y.; Zhao, Z.; Chen, J.; Yang, T.; Cremer, P. S. Deflected capillary force lithography. *ACS Nano* **2012**, *6*, 1548−1556.